UNIVERSITÄT AUGSBURG
Universitätsbibliothek

OPEN ACCESS
OPUS AUGSBURG

Thermochromic modulation of surface plasmon polaritons in vanadium dioxide nanocomposites

Thorben Jostmeier, Hans Moritz Mangold, Johannes Zimmer, Helmut Karl, Hubert J. Krenner, Claudia Ruppert, Markus Betz

Angaben zur Veröffentlichung / Publication details:

Jostmeier, Thorben, Hans Moritz Mangold, Johannes Zimmer, Helmut Karl, Hubert J. Krenner, Claudia Ruppert, and Markus Betz. 2016. "Thermochromic modulation of surface plasmon polaritons in vanadium dioxide nanocomposites." *Optics Express* 24 (15): 17321–31. https://doi.org/10.1364/OE.24.017321.

Nutzungsbedingungen / Terms of use:

licgercopyright

Dieses Dokument wird unter folgenden Bedingungen zur Verfügung gestellt: / This document is made available under these conditions:
Deutsches Urheberrecht
Weitere Informationen finden Sie unter: / For more information see:
https://www.uni-augsburg.de/de/organisation/bibliothek/publizieren-zitieren-archivieren/publiz/

Research Article | Vol. 24, No. 15 | 25 Jul 2016 | OPTICS EXPRESS 17321

Optics EXPRESS

Thermochromic modulation of surface plasmon polaritons in vanadium dioxide nanocomposites

THORBEN JOSTMEIER,[1,*] MORITZ MANGOLD,[2,3] JOHANNES ZIMMER,[2,3] HELMUT KARL,[4] HUBERT J. KRENNER,[2,3] CLAUDIA RUPPERT,[1] AND MARKUS BETZ[1]

[1]*Experimentelle Physik 2, TU Dortmund University, 44227 Dortmund, Germany*
[2]*Lehrstuhl für Experimentalphysik I and Augsburg Centre for Innovative Technologies (ACIT), Universität Augsburg, 86159 Augsburg, Germany*
[3]*Nanosystems Initiative Munich (NIM), 80799 München, Germany*
[4]*Lehrstuhl für Experimentalphysik IV, Universität Augsburg, 86159 Augsburg, Germany*
*thorben.jostmeier@tu-dortmund.de

Abstract: We propose and implement a new concept for thermochromic plasmonic elements. It is based on vanadium dioxide (VO_2) nanocrystals located in the near field of surface plasmon polaritons supported by an otherwise unstructured gold thin film. When the VO_2 undergoes the metal-insulator phase transition, the coupling conditions for conversion of light into propagating surface plasmon polaritons change markedly. In particular, we realize thermochromic plasmonic grating couplers with substantial switching contrast as well as tunable plasmonic couplers in a Kretschmann configuration. The use of VO_2 nanocrystals permits highly repetitive switching and room temperature operation. Simulations based on the actual dielectric function of our VO_2 nanocrystals agree well with the experiment.

© 2016 Optical Society of America

OCIS codes: (050.6624) Subwavelength structures, (130.4110) Modulators, (160.6840) Thermo-optical materials, (240.6680) Surface plasmons, (250.5403) Plasmonics.

References and links

1. J. D. Cox and F. Javier García de Abajo, "Electrically tunable nonlinear plasmonics in graphene nanoislands," Nat. Commun. **5**, 5725 (2014).
2. C. Ruppert, F. Föster, A. Zrenner, J. B. Kinzel, A. Wixforth, H. J. Krenner, and M. Betz, "Radio frequency electromechanical control over a surface plasmon polariton coupler," ACS Photon. **1**, 91–95 (2014).
3. J. Schiefele, J. Pedrós, F. Sols, F. Calle, and F. Guinea, "Coupling light into graphene plasmons through surface acoustic waves," Phys. Rev. Lett. **111**, 237405 (2013).
4. N. Rotenberg, M. Betz, and H. M. van Driel, "Ultrafast control of grating-assisted light coupling to surface plasmons," Opt. Lett. **33**, 2137–2139 (2008).
5. K. F. MacDonald, Z. L. Samson, M. I. Stockman, and N. I. Zheludev, "Ultrafast active plasmonics," Nat. Photon. **3**, 55–58 (2009).
6. F. J. Morin, "Oxides which show a metal-to-insulator transition at the Neel temperature," Phys. Rev. Lett. **3**, 34–36 (1959).
7. A. Zylbersztejn and N. F. Mott, "Metal-insulator transition in vanadium dioxide," Phys. Rev. B **11**, 4383–4395 (1975).
8. H. W. Verleur, A. S. Barker, Jr, and C. N. Berglund, "Optical properties of VO_2 between 0.25 and 5 eV," Phys. Rev. **172**, 788–798 (1968).
9. M. Tazawa, P. Jin, and S. Tanemura, "Optical constants of $V_{1-x}W_xO_2$ films," Appl. Opt. **37**, 1858–1861 (1998).
10. J. Zimmer, A. Wixforth, H. Karl, and H. J. Krenner, "Ion beam synthesis of nanothermochromic diffraction gratings with giant switching contrast at telecom wavelengths," Appl. Phys. Lett. **100**, 231911 (2012).
11. T. Jostmeier, J. Zimmer, H. Karl, H. J. Krenner, and M. Betz, "Optically imprinted reconfigurable photonic elements in a VO_2 nanocomposite," Appl. Phys. Lett. **105**, 071107 (2014).
12. T. V. Son, C. O. F. Ba, R. Vallée, and A. Haché, "Nanometer-thick flat lens with adjustable focus," Appl. Phys. Lett. **105**, 231120 (2014).
13. X.-Y. Peng, B. Wang, J. Teng, J. B. Kana Kana, and X. Zhang, "Active near infrared linear polarizer based on VO_2 phase transition," J. Appl. Phys. **114**, 163103 (2013).
14. D. Wang, L. Zhang, Y. Gu, M. Q. Mehmood, Y. Gong, A. Srivastava, L. Jian, T. Venkatesan, C.-W. Qiu, and M. Hong, "Switchable ultrathin quarter-wave plate in terahertz using active phase-change metasurface," Sci. Rep. **5**, 15020 (2015).

#265054 http://dx.doi.org/10.1364/OE.24.017321
Journal © 2016 Received 12 May 2016; revised 24 Jun 2016; accepted 5 Jul 2016; published 21 Jul 2016

Optics EXPRESS

15. J. Rensberg, S. Zhang, Y. Zhou, A. S. McLeod, C. Schwarz, M. Goldflam, M. Liu, J. Kerbusch, R. Nawrodt, S. Ramanathan, D. N. Basov, F. Capasso, C. Ronning, and M. A. Kats, "Active optical metasurfaces based on defect-engineered phase-transition materials," Nano Lett. **16**, 1050–1055 (2016).
16. R. M. Briggs, I. M. Pryce, and H. A. Atwater, "Compact silicon photonic waveguide modulator based on the vanadium dioxide metal-insulator phase transition," Opt. Express **18**, 11192–11201 (2010).
17. J. D. Ryckman, K. A. Hallman, R. E. Marvel, R. F. Haglund, Jr., and S. M. Weiss, "Ultra-compact silicon photonic devices reconfigured by an optically induced semiconductor-to-metal transition," Opt. Express **21**, 10753–10763 (2013).
18. K. Appavoo and R. F. Haglund, Jr., "Polarization selective phase-change nanomodulator," Sci. Rep. **4**, 6771 (2014).
19. J. Y. Suh, E. U. Donev, R. Lopez, L. C. Feldman, and R. F. Haglund, Jr., "Modulated optical transmission of subwavelength hole arrays in metal-VO_2 films," Appl. Phys. Lett. **88**, 133115 (2006).
20. L. A. Sweatlock and K. Diest, "Vanadium dioxide based plasmonic modulators," Opt. Express **20**, 8700–8709 (2012).
21. Y. Sharma, V. A. Tiruveedhula, J. F. Muth, and A. Dhawan, "VO_2 based waveguide-mode plasmonic nano-gratings for optical switching," Opt. Express **23**, 5822–5849 (2015).
22. D. Y. Lei, K. Appavoo, F. Ligmajer, Y. Sonnefraud, R. F. Haglund, Jr., and S. A. Maier, "Optically-triggered nanoscale memory effect in a hybrid plasmonic-phase changing nanostructure," ACS Photon. **2**, 1306–1313 (2015).
23. J. Jeong, A. Joushaghani, S. Paradis, D. Alain, and J. K. S. Poon, "Electrically controllable extraordinary optical transmission in gold gratings on vanadium dioxide," Opt. Lett. **40**, 4408–4411 (2015).
24. P. Markov, K. Appavoo, R. F. Haglund, Jr., and S. M. Weiss, "Hybrid Si-VO_2-Au optical modulator based on near-field plasmonic coupling," Opt. Express **23**, 6878–6887 (2015).
25. B. A. Kruger, A. Joushaghani, and J. K. S. Poon, "Design of electrically driven hybrid vanadium dioxide (VO_2) plasmonic switches," Opt. Express **20**, 23598–23609 (2012).
26. A. Joushaghani, B. A. Kruger, S. Paradis, D. Alain, J. Stewart Aitchison, and J. K. S. Poon, "Sub-volt broadband hybrid plasmonic-vanadium dioxide switches," Appl. Phys. Lett. **102**, 061101 (2013).
27. M. Beebe, L. Wang, S. E. Madaras, J. M. Klopf, Z. Li, D. Brantley, M. Heimburger, R. A. Wincheski, S. Kittiwatanakul, J. Lu, S. A. Wolf and R. A. Lukaszew, "Surface plasmon resonance modulation in nanopatterned Au gratings by the insulator-metal transition in vanadium dioxide films," Opt. Express **23**, 13222–13229 (2015).
28. S. K. Earl, T. D. James, T. J. Davis, J. C. McCallum, R. E. Marvel, R. F. Haglund, and A. Roberts, "Tunable optical antennas enabled by the phase transition in vanadium dioxide," Opt. Express **21**, 27503–27508 (2013).
29. M. A. Kats, R. Blanchard, P. Genevet, Z. Yang, M. M. Qazilbash, D. N. Basov, S. Ramanathan, and F. Capasso, "Thermal tuning of mid-infrared plasmonic antenna arrays using a phase change material," Opt. Lett. **38**, 368–370 (2013).
30. J. He, Z. Xie, W. Sun, X. Wang, Y. Ji, S. Wang, Y. Lin, and Y. Zhang, "Terahertz tunable metasurface lens based on vanadium dioxide phase transition," Plasmonics 1–6 (2016).
31. Z. L. Sámson, K. F. MacDonald, F. De Angelis, B. Gholipour, K. Knight, C. C. Huang, E. Di Fabrizio, D. W. Hewak, and N. I. Zheludev, "Metamaterial electro-optic switch of nanoscale thickness," Appl. Phys. Lett. **96**, 143105 (2010).
32. A.-K. U. Michel, D. N. Chigrin, T. W. W. Maß, K. Schönauer, M. Salinga, M. Wuttig, and T. Taubner, "Using low-loss phase-change materials for mid-infrared antenna resonance tuning," Nano Lett. **13**, 3470–3475 (2013).
33. T. Hira, T. Homma, T. Uchiyama, K. Kuwamura, and T. Saiki, "Switching of localized surface plasmon resonance of gold nanoparticles on a GeSbTe film mediated by nanoscale phase change and modification of surface morphology," Appl. Phys. Lett. **103**, 241101 (2013).
34. T. Cao, C. Wei, R. E. Simpson, L. Zhang, and M. J. Cryan, "Fast tuning of double Fano resonance using a phase-change metamaterial under low power intensity," Sci. Rep. **4**, 4463 (2014).
35. M. Rudé, R. E. Simpson, R. Quidant, V. Pruneri, and J. Renger, "Active control of surface plasmon waveguides with a phase change material," ACS Photon. **2**, 669–674 (2015).
36. M. Rini, A. Cavalleri, R. W. Schoenlein, R. López, L. C. Feldman, R. F. Haglund, Jr., L. A. Boatner, and T. E. Haynes, "Photoinduced phase transition in VO_2 nanocrystals: ultrafast control of surface-plasmon resonance," Opt. Lett. **30**, 558–560 (2005).
37. R. Lopez, L. A. Boatner, T. E. Haynes, L. C. Feldman, and R. F. Haglund, Jr., "Synthesis and characterization of size-controlled vanadium dioxide nanocrystals in a fused silica matrix," J. Appl. Phys. **92**, 4031–4036 (2002).
38. H. Kakiuchida, P. Jin, S. Nakao and M. Tazawa "Optical properties of vanadium dioxide film during semiconductive-metallic phase transition," Jap. J. Appl. Phys. **46**, L113 (2007).
39. R. Lopez, L. Feldman, and R. F. Haglund, Jr., "Size-dependent optical properties of VO_2 nanoparticle arrays," Phys. Rev. Lett. **93**, 177403 (2004).
40. H. Raether, *Surface plasmons on smooth and rough surfaces and on gratings*, (Springer, 1988).
41. P. B. Johnson and R. W. Christy, "Optical constants of the noble metals," Phys Rev B **6**, 4370–4379 (1972).
42. I. H. Malitson, "Interspecimen comparison of the refractive index of fused silica," J Opt Soci Am **55**, 1205–1209 (1965).
43. E. Kretschmann, "Die Bestimmung optischer Konstanten von Metallen durch Anregung von Oberflächenplasmaschwingungen," Zeitschrift für Physik **241**, 313–324 (1971).

Optics EXPRESS

1. Introduction

Surface plasmon polaritons (SPPs) are collective electronic excitations propagating along a metal-dielectric interface and play a key role in various scientific areas. In particular, the controlled coupling of free-space radiation into SPPs is integral to developments in nanophotonics. The emerging area of "active plasmonics" focuses on fast and deterministic control of plasmonic devices. So far, most concepts have relied on electrical [1] , electro-mechanical [2,3] or (ultrafast) optical manipulations [4, 5], of the SPP launching and/or propagation. In essence, such optical approaches rely on the modification of the dielectric function associated with the photoexcitation. However, even more substantial changes to the dielectric properties can be induced by structural phase transitions. In this context, vanadium dioxide (VO_2) attracts extensive interest as it exhibits a metal-insulator phase transition (MIT) close to ambient temperatures ($\approx 68^\circ$C for bulk crystals). Upon heating, VO_2 undergoes a structural change from a room temperature insulating to a high temperature metallic phase [6, 7]. In particular, this MIT is accompanied by a marked change of the complex dielectric function in the telecom window [8, 9]. Several photonic elements employing this control mechanism have been demonstrated or proposed, comprising nanoscale diffraction gratings [10, 11] and lenses [11, 12], polarization optics [13–15] or photonic modulators [16–18]. Recent studies have also been devoted to the use of VO_2 for modulating plasmonic functionalities [19–24], including the propagation of SPPs [25–27] and antenna resonances [28–30]. In addition, similar concepts have been demonstrated based on other phase change materials [31–35]. However, the benefit of VO_2 for active control of SPP launching in plain metal films has not been addressed so far.

In this Letter we optically investigate plasmonic elements with VO_2 nanocrystals (NCs) embedded just below the surface of a gold covered dielectric. The phase transition in these VO_2-NCs can be conveniently induced by (local) heating and/or optical excitation. In addition, it exhibits a large hysteresis with a supercooled metallic state at ambient temperatures. The bistability of nanoscale VO_2 specimen allows for the implementation of persistent, but erasable photonic elements [11] or plasmonic memory devices [22]. Owing to a Mie-type resonance of the spherical metallic NCs, the change of the dielectric function during the MIT is strongly increased compared to bulk films [36]. Furthermore, the spectral position of this resonance and the characteristics of the hysteresis can be engineered during the fabrication process.

For well-defined SPP launching, two main mechanisms have been identified. In one approach, the momentum transfer related to spatially periodic structures helps to overcome the momentum mismatch between free-space radiation and SPPs propagating on a metal surface. Alternatively, the evanescent field associated with total internal reflection is able to excite SPPs in the Kretschmann configuration. To demonstrate the usefulness of the MIT in VO_2 for tunable SPP launching, we investigate nanocomposite samples following those two approaches: (i) By site-selective deactivation of the phase transition in the NCs, we form thermochromic diffraction gratings. When covered with gold thin films, these specimens act as thermochromic plasmonic grating couplers with substantial switching contrast. (ii) Another set of experiments addresses Kretschmann configurations with VO_2-NCs in the optical near field of propagating SPPs. Here, a marked change of the coupling angle of such a SPP launcher is observed when the NCs undergo the phase transition. All the findings are in line with measurements of the actual dielectric function of the VO_2-NCs in the insulating and metallic regime.

2. Sample characterization

Our samples consist of a dense layer of unconnected VO_2-NCs embedded in fused silica (SiO_2). The NCs are synthesized by sequential ion beam implantation of vanadium ($9 \times 10^{16}/\text{cm}^2$, 100 keV) and oxygen ($1.8 \times 10^{17}/\text{cm}^2$, 36 keV) followed by a 10 min rapid thermal annealing step at 1000°C [10,37]. The resulting VO_2-NCs are approximately spherical and are characterized

Optics EXPRESS

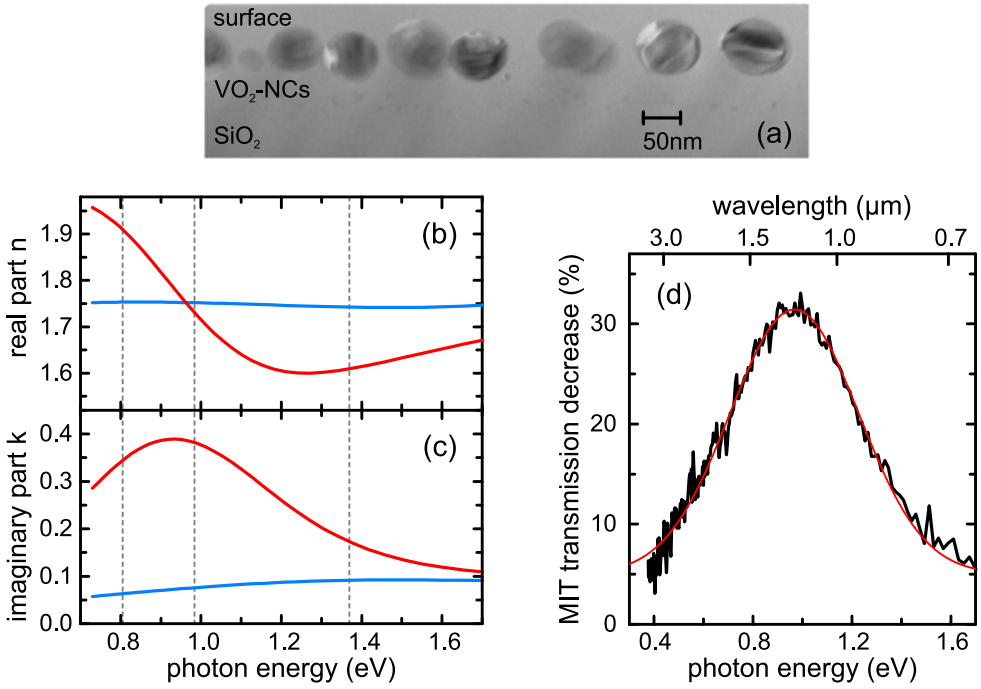

Fig. 1. (a) Cross-section transmission electron microscope image of ion beam synthesized VO_2 nanocrystals (NCs) embedded in a fused silica matrix. (b) Real and (c) imaginary part of the refractive index of the VO_2 nanocrystal (NC) layer as determined by ellipsometry for different sample temperatures. Blue: 28°C (insulating). Red: 100°C (metallic). The vertical dashed lines indicate the photon energies used for the plasmonic switching. (d) Decrease of optical transmissivity related to the phase transition from insulating to metallic VO_2-NCs. The red line is a Gaussian fit to the data.

by an average diameter of 90 nm and an areal density of $\sim 1 \times 10^{10}\mathrm{cm}^{-2}$. They are centered 85nm below the surface. A typical transmission electron micrograph is shown in Fig. 1(a). Unlike most bulk or thin-film VO_2 specimen, the NCs allow for highly repepetive switching without any structural desintegration [11]. The guiding idea of our study is to functionalize such specimens with gold thin films such that the VO_2-NCs are located in the near-field of SPPs supported by this metal film. As a consequence, SPP launching and/or propagation can be modulated exploiting the MIT of VO_2.

We first address the change of the complex refractive index function of the VO_2-NCs during the MIT. To this end, we perform spectral ellipsometry on an unprocessed VO_2-NCs:SiO_2 sample and analyze the real and imaginary part of the refractive index $\tilde{n} = n + ik$ of the VO_2-NC layer, cf. Figs. 1 (b) and 1(c). For the NC layer, we use an effective medium approach with spherical VO_2-NCs embedded in SiO_2. For the dielectric function of VO_2, we employ an established model with three Lorentz oscillators [38]. Close to room temperature, all NCs are in the insulating phase and the spectral signature is rather flat. At elevated temperatures above the MIT, the NCs are in the metallic phase. The optical response is now governed by a Mie-type resonance within the metallic VO_2-NCs. It is adaequately described by Mie theory for the polarizability of spherical particles [36, 39]. This resonance results in a strongly increased imaginary part k and a dispersive signature in the real part n. For further characterization, we perform spectrally resolved transmission measurements at normal incidence. Due to the increased imaginary part k the transmission is reduced by >30% in the metallic phase despite an effective interaction

Optics EXPRESS

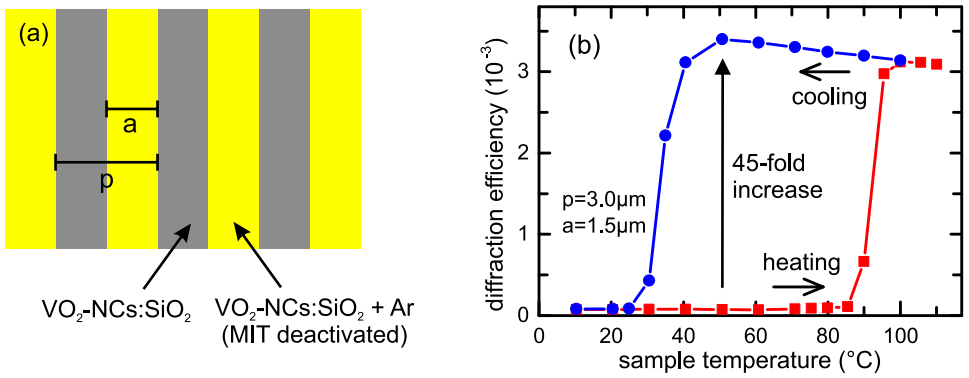

Fig. 2. (a) Schematic top view of the grating structures fabricated by site-selective deactivation of the metal-insulator phase transition (MIT) using implantation of Ar^+ ions. (b) First order diffraction efficiency of $\lambda = 1.55\mu$m light (normal incidence) for various sample temperatures during heating (red quares) and cooling cycles (blue circles).

length of < 50 nm, cf. Fig. 1(d). The spectrum of the transmission change is well described by a Gaussian centered at 0.97 eV, reflecting the Mie-type resonance in the NCs. We note that throughout the paper we investigate two VO_2-NC samples which slightly differ in resonance shape and absorption strength. This does not affect the main conclusions below.

3. Plasmonic grating couplers

We now turn towards the demonstration of a switchable SPP launcher based on a thermochromic grating which utilizes the change of the VO_2 dielectric function during the MIT. To this end, we define grating patterns in the VO_2-NC layer via site-selective deactivation of the MIT. Details of the procedure are described in [10]. In short, the grating profile is defined by e-beam lithography. Then we irradiate the sample with Ar^+ ions ($7 \times 10^{15}/\text{cm}^2$, 80 keV) such that point defects are introduced into the NCs located in uncovered areas. As a result, the MIT is inhibited such that the deactivated NCs do not switch to the metallic phase irrespective of heating and/or optical excitation. It has already been shown that the dielectric contrast between the regular and deactivated NCs can be utilized to create thermochromic diffraction gratings [10], tunable polarizers [15] and other reconfigurable photonic elements [11].

For the aim of plasmonic grating couplers, we apply the site-selective deactivation procedure and form $\sim 500\mu m$ large gratings of different periodicities p and duty cycles a/p, cf. sketch in Fig. 2(a). For characterization purposes, we measure their first order diffraction efficiency in transmission geometry while driving the MIT. The samples are mounted on a temperature-controlled holder. Two goniometer stages allow us to independently tune the angle of incidence and the detection angle. As a light source, a commercial femtosecond Er:fiber laser (Toptica FFS) is used. An optical bandpass filter centered at 1.55μm (0.8eV) narrows its output spectrum to 15nm width (FWHM). The use of pulsed optical sources as opposed to cw-lasers is chosen simply because of the availability in our lab. In Fig. 2(b), the intensity of the first order diffraction, normalized to the intensity transmitted at 10°C, is plotted for various sample temperatures. Below a critical temperature T_C, all NCs are in the insulating phase. Upon heating, the steep rise of the diffracted signal at $T_C \approx 90$°C is caused by the MIT. Above T_C, the alternating areas of insulating (deactivated) and metallic VO_2 act as a diffraction grating. When cooling the sample again a supercooled metallic phase persists down to ~ 35°C. When the temperature is reduced further the NCs switch back to the insulating phase. As a consequence, the dielectric contrast vanishes and the diffraction efficiency approaches its initial small value. The marked

Optics EXPRESS

thermal hysteresis can be attributed to the first order phase transition and the good crystallinity of the single-domain NCs and surrounding SiO_2 matrix [11]. Remarkably, the almost complete absence of a dielectric contrast between deactivated and insulating VO_2 results in a substantial switching contrast. Specifically, the diffraction efficiency in the supercooled state exceeds that of the insulating state by a factor of ~ 45.

To enable the plasmonic functionality of these gratings, a 2nm thick titanium adhesion layer and a nominally 25nm thick gold layer are deposited on top of the grating patterns. We focus on the SPP modes supported at the air-gold interface. Related to the thin metal film, these surface-bound modes partly overlap with the NC layer, cf. Fig. 3(a) for visualization. It is well known that the dispersion relation of SPPs at a metal-air interface reads

$$k_{\mathrm{SPP}} = k_0 \sqrt{\frac{\epsilon_{\mathrm{m}}}{\epsilon_{\mathrm{m}} + 1}} \tag{1}$$

where ϵ_m is the dielectric functions of the metal (for air, $\epsilon_d \approx 1$) and $k_0 = 2\pi/\lambda$ is the free-space vector of light. A widely used method to overcome the momentum mismatch with respect to incident free-space radiation is the grating-induced SPP coupling. In particular, TM polarized light with an off-normal angle of incidence θ can be converted into propagating SPPs whenever the condition

$$k_{\mathrm{SPP}} = k_0 \sin(\theta) \pm m K_G \tag{2}$$

with $K_G = 2\pi/p$, the grating period p and an integer m is fulfilled [40].

To verify SPP launching, we investigate the angular dependence of the optical transmission for insulating and supercooled metallic VO_2-NCs. The light source is again a pulsed Er:fiber laser centered at 0.8 eV. In order to ensure sufficient angular resolution, we loosely focus its output to form ~100 μm spots on the grating. As SPP excitation is only possible for TM polarized light, we directly measure the difference in transmissivity of TM and TE polarized light using a polarizing beam splitter, two InGaAs photodiodes and the differential input of a lock-in amplifier referenced to the laser output. Via this detection scheme, the increased absorption in the metallic phase does not contribute to the signal. Figure 3(b) shows the angular dependence of the difference of TM and TE transmissivity for a grating with $p = 2.5\,\mu m$ in the insulating and supercooled metallic state. The sample temperature of 50°C is the same in both cases. To prepare the supercooled metallic phase, we make use of the thermal hysteresis of the MIT in the NCs. The samples are heated to 105°C and subsequently cooled down to 50°C. As a consequence, our procedure separates the influence of the MIT from any other thermal effect that might occur in the nanocomposite. Owing to the different angular dependences of the Fresnel coefficients at the various interfaces, the signals in Fig. 3(b) show an overall slope. More importantly, a distinct signature of SPP launching is evident at an angle of incidence of $\approx 23°$. This resonance is clearly seen in the data in Fig. 3(c) where we subtract the slowly varying background. When the grating in the VO_2 layer is activated by switching to the metallic phase, the coupling condition (2) is fulfilled. The sub-wavelength proximity of the gold-air interface to the NC layer ensures a spatial overlap with the SPP modes (see Fig. 3(a) for an illustration). As a result, a fraction of the TM polarized incident light is converted to SPPs and, thus, the differential transmission decreases. The maximum signal strengths in Fig. 3(c) point towards an efficiency of SPP launching of ~ 0.5%, i.e., similar to the diffraction efficiencies seen in Fig. 2.

To corroborate our interpretation, we calculate the resonance angle using the Eqs. (1) and (2) with $m = 1$ and literature data for the dielectric function of gold [41] and SiO_2 [42]. The vertical arrow in Fig. 3(c) marks the calculated positions and agrees very well with the observed resonance angle. When all the VO_2-NCs are in the insulating phase, only a small dispersive feature is seen, reflecting the residual dielectric contrast between Ar-exposed and as-grown NCs.

We also analyze the influence of the duty cycle a/p of the grating in a range from 0.2 from 0.6 (data not shown). MIT-induced SPP resonances are found for all gratings. The coupling

Optics EXPRESS

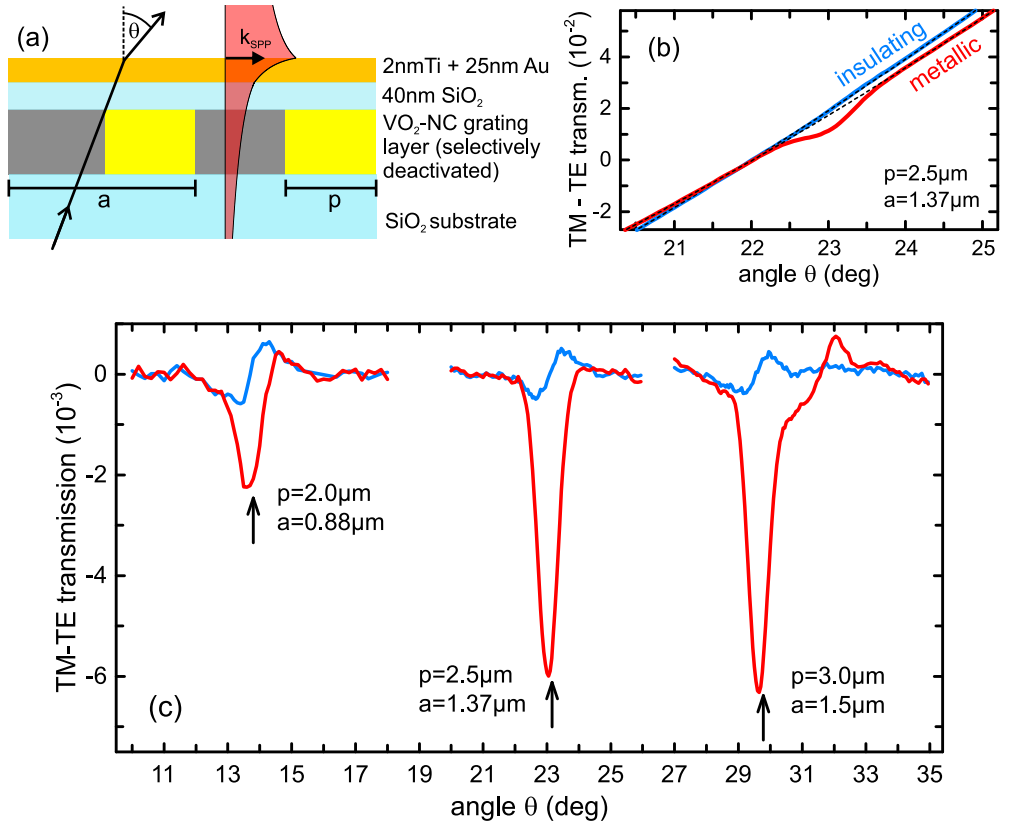

Fig. 3. (a) Schematic cross-section of a gold covered VO_2 nanocrystal (NC) sample featuring alternating stripes of deactivated and as-grown NCs. The red area illustrates the field distribution of surface plasmon polaritions (SPPs), launched at $\lambda = 1.55\mu m$ (black line). (b) Difference of TM and TE polarized transmission for insulating (blue) and metallic (red) VO_2-NCs in the as-grown areas. Dashed lines are parabolic fits to the background signals. (c) Background-corrected transmission data for different grating periods. The vertical arrows mark the expected SPP resonance positions.

efficiency is largest for ~0.5 duty cycle, as is the diffraction efficiency.

To further confirm our signals as arising from thermochromic SPP resonances, we investigate samples with different grating period p. Figure 3(c) also includes the background-corrected data for $p = 2.0\,\mu m$ and $p = 3.0\,\mu m$. The resonance angle is seen to markedly shift with the grating period. Again, the vertical arrows indicate the expected positions which are fully in line with the experiment. In all investigated samples with site-selective deactivation of the MIT, the large dielectric switching contrast of the gratings ensures a practically complete on-off modulation of the SPP resonance. When the sample temperature is decreased to room temperature, the grating pattern is erased in a non-destructive fashion and the plasmonic grating coupler is switched off.

4. Kretschmann configuration

In a second set of experiments, we investigate the influence a VO_2-NC layer on the coupling of SPPs in the Kretschmann geometry [40, 43]. In this configuration, matching the in-plane momentum of the incident light to the SPP, cf. Eq. (1) is achieved by effectively increasing the light's wave vector in a dielectric with refractive index $n_s > 1$. Thereby, the restriction $k_{SPP} > k_0$

Optics EXPRESS

is removed and the new coupling condition reads:

$$k_{\mathrm{SPP}} = n_{\mathrm{s}} \sin(\theta) k_0 \ . \tag{3}$$

The sample geometry used to implement this configuration is depicted in Fig. 4(a). The dielectric is fused silica, i.e. $n_{\mathrm{s}} = n_{\mathrm{fs}} \approx 1.44$. Most importantly, the prism enables the angle θ to become large enough to fulfill Eq. (3). This equation determines the angle θ where TM polarized light potentially launches SPPs at the gold-air interface. When the coupling condition is fulfilled, energy is transferred from incident light to SPP modes and, thus, the optical reflectivity is reduced for a specific angle.

We now investigate how the light-SPP conversion is affected by change of the dielectric function of the nearby VO_2-NC layer during the MIT. To this end, we detect the reflectivity R_{TM} for TM polarized light in the setup described above and vary the angle of incidence. As a light source we use an optical parametric amplifier (Coherent OPA 9850) in combination with a bandpass (12nm FWHM) centered at a wavelength of 1.26μm (0.98 eV photon energy). For this photon energy, only the imaginary part of the VO_2-NC's refractive index is affected by the MIT, cf. Fig. 1. In Fig. 4(b), this angular dependence of R_{TM} is displayed for insulating VO_2-NCs (65°C sample temperature, blue line). Note that we normalize the signal to $R_{\mathrm{TM}}(\theta = 43.0°) = 1$. While the rise of the signal at $\theta \approx 43.8°$ is due to the onset of total internal reflection, it is followed by a rapid decrease related to a resonance where the evanescent light launches SPPs. At the resonance peak at $\theta = 44.2°$, the reflectivity of the structure is as small as ~10% and, therefore, most of the incident light is transferred to SPP modes. In the metallic phase at the same temperature (red line), the overall reflectivity R_{TM} is reduced by roughly a factor of two. This reduction arises from the double pass through the VO_2-NC layer and agrees well with the transmission data in Fig. 1(c). More importantly, the resonance broadens and shifts to a slightly larger angle. This result may be explained by the increased damping related to increasing losses in the metallic VO_2-NCs. The altered shape of the resonance becomes more evident when the reflectivity is again normalized to $R_{\mathrm{TM}}(\theta = 43.0°) = 1$ (red dashed line).

For a more detailed analysis of the MIT-induced changes to the SPP resonance, we repeat the Kretschmann type experiments for different photon energies. In particular, the nature of the MIT in our VO_2-NCs opens up the possibility to select photon energies where the real part of the dielectric function increases (0.8 eV), remains unchanged (0.98 eV) or decreases (1.37 eV). Note that the imaginary part always increases, cf. Fig. 1. In addition to the two light sources above, a home-built Ti:sapphire laser in combination with a 10nm (FWHM) wide bandpass at 0.905μm (1.37 eV) is employed. In Figs. 5(a)-5(c) the MIT-induced change of the reflectance is shown for the three photon energies (red lines). While the overall offset is again related to the transmission decrease related to the double pass through the VO_2-NC layer, the MIT-induced change to the SPP resonance results in markedly different angular shapes. In particular, the effect of the MIT on the reflectivity $R_{\mathrm{TM}}(\theta)$ is remarkably sensitive to the angle of incidence. For example, at 0.98 eV photon energy, the change in reflectance varies from 30% to 80% within an angular range as small as 0.05°.

Finally we aim to quantitatively model the influence of the MIT on the plasmonic resonance. At the same time, we elucidate the role of real and imaginary part of the dielectric function of the VO_2-NCs. To this end, we simulate the optical response of the Kretschmann geometry using a transfer-matrix method. Specifically, the simulations compute the TM reflectivity for varying angles of incidence ($R_{\mathrm{TM}}(\theta)$). The sample is modeled by a five layer sequence, with air and fused silica as the semi-infinite top and bottom layer, respectively. The VO_2-NCs are taken into account as a homogeneous layer with a thickness of 90 nm. The real part of the refractive index is taken from the actual ellipsometry data in Fig. 1(a). The imaginary part is adjusted such that the transmission decrease far away from the resonance is reproduced by the simulations (we note that this procedure results in a better agreement as the NCs used for the Kretschmann

Optics EXPRESS

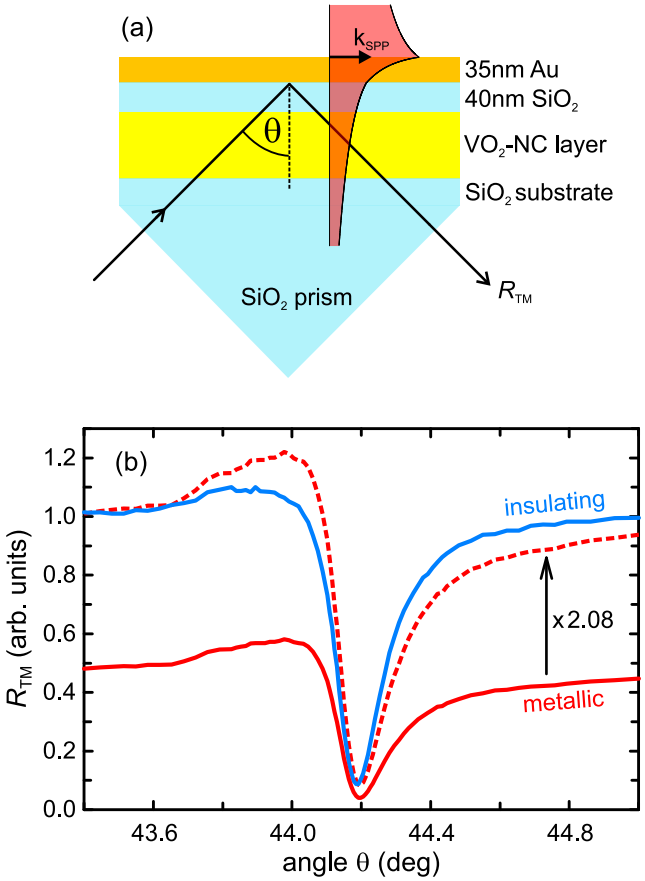

Fig. 4. (a) Schematic cross-section of the sample geometry used in the Kretschmann configuration. TM polarized light (black line) is incident on a fused silica prism attached to a gold covered VO_2 nanocrystal (NC) sample. The red area illustrates the field distribution of surface plasmon polaritons. (b) Reflectivity data $R_{TM}(\theta)$ for insulating (blue line) and metallic (red line) VO_2-NCs together with normalized metallic phase data (red dashed line).

type experiments slightly differ from those used to obtain the ellipsometry data). The refractive indices of gold [41] and fused silica [42] are taken from literature.

In a first step, we selectively change only either the real n or imaginary part k of the refractive index $\tilde{n} = n + ik$ and simulate $R_{TM}(\theta)$ for the photon energies used in the experiment. The resulting data are shown in Figs. 5(d)-5(f). The main finding is that the shift and the broadening of the resonance are determined by the increased imaginary part, which leads to increased damping of the SPPs in the VO_2 layer. In contrast, a modification of the real part n primarily changes the overall reflectivity of the structure. Remarkably, it also leads to a deeper resonance at photon energies of 0.80 eV and 1.37 eV. This finding is related to the destructive interference of (totally) reflected light with light that is re-emitted from SPPs into the substrate. This interference determines the minimum reflectivity in the Kretschmann configuration [40]. The phase shift introduced by the change in n modifies this interference. In our sample configuration, the reflectivity is close to being minimal for 0.98 eV photon energy and insulating VO_2 and, thus, the MIT leads to a slightly reduced resonance strength. In contrast, at both 0.80 eV and 1.37 eV photon energy, the phase shift induced by the altered real part improves the destructive interference when switching to the metallic phase.

Optics EXPRESS

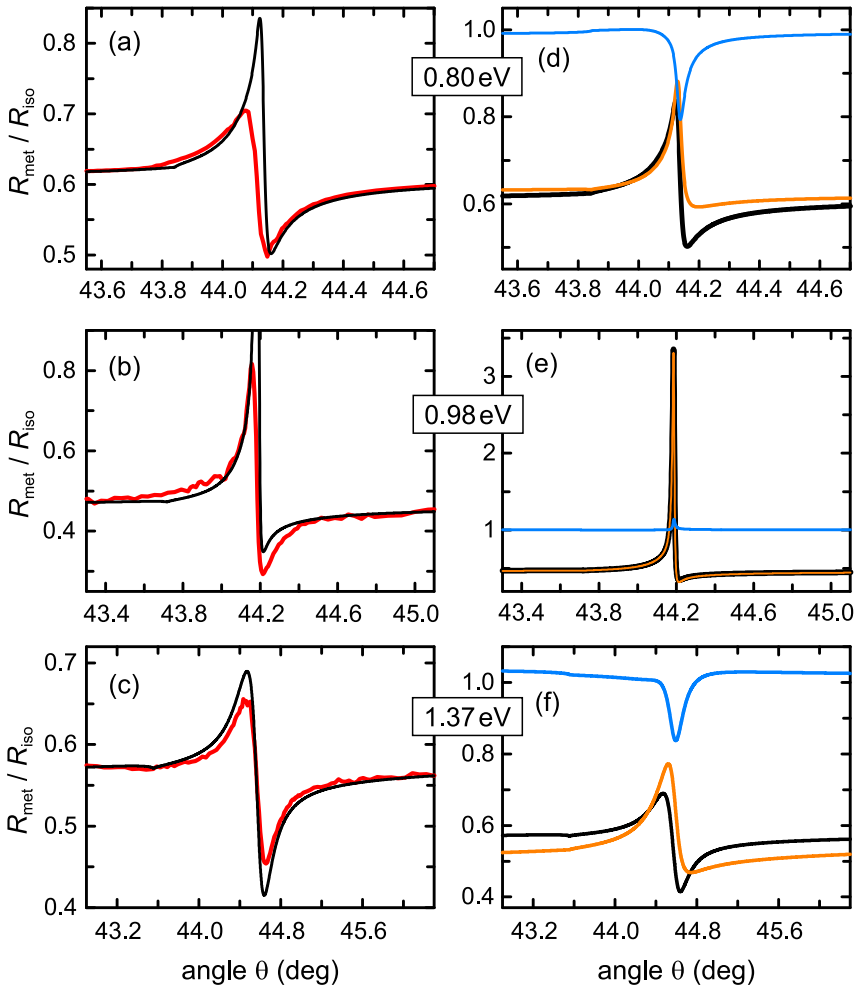

Fig. 5. Change of the reflectance of TM polarized light in the Kretschmann configuration caused by the phase transition from insulating to metallic VO_2 for different photon energies. (a)-(c) Experimental data (red lines) and results of simulations based on the transfer-matrix method (black lines). (d)-(f) Simulation results for a change of either only the imaginary or only the real part of the VO_2 refractive index $\tilde{n} = n + ik$. Blue lines reflect the change in the real part of the dielectric function while the orange lines originate from the change in the imaginary part. Black lines show simulations for the full change of the dielectric function which are also contained in panels (a) - (c).

Optics EXPRESS

A full understanding of the MIT-induced change to the SPP coupling requires to incorporate both the real and the imaginary part of the dielectric function. In Figs. 5(a)-5(f), the results of these full simulations are included as black lines. It is evident that the influence of the VO_2-NC layer on the SPP resonance is well reproduced by the simulations. In particular, the positions of the resonance coincide and the angular shapes of the MIT-induced changes match the experimental results. The remaining deviations are likely related to the finite spectral and angular resolution of the experiment and, to some extent, to the uncertainty in the refractive index data.

5. Conclusion

To summarize, we have demonstrated a new class of plasmonic elements that takes full advantage of the optical bistability and the substantial changes of the near-infrared polarizability of VO_2 nanocrystals undergoing a metal-insulator phase transition. Paradigmatic examples comprise thermochromic plasmonic grating couplers and thermo-tunable SPP launchers in a Kretschmann configuration. The structures offer substantial modulations close to room temperature and exhibit a pronounced hysteresis. We note that doping of the VO_2 nanocrystals enables to further taylor the structural transition. So far, we have focused on a purely thermal modulation at room temperature. However, it is well known that the phase transition in VO_2 can also be optically triggered on sub-ps timescales. As a result, the concept can be easily extended to modulations at GHz frequencies.

Acknowledgment

We acknowledge financial support by the Deutsche Forschungsgemeinschaft (DFG) in the framework of the collaborative research center SFB TRR 142. H.J.K., J.Z. and M.M. acknowledge support by the DFG through the Emmy-Noether program.

137.250.100.44 {ts '2019-11-20 07:58:07'}